

Mitigation of textile industries generated pollution by agro-waste cotton peels mediated synthesized silver nanoparticles

Boya Palajonna Narasaiah¹, Badal Kumar Mandal^{1,*}, Sarada Nallani Chakravarthula¹

¹Department of Chemistry, School of Advanced Sciences, Vellore Institute of Technology (VIT), Vellore 632014, Tamil Nadu, India

*corresponding author e-mail address: badalmandal@vit.ac.in

ABSTRACT

The present study reports the synthesis of silver nanoparticles (Ag NPs) by using empty cotton boll peels (ECBP) aqueous extract. The formation of Ag NPs was confirmed by its surface Plasmon resonance (SPR) band at 432 nm using a UV-visible spectrophotometer. The phase purity and crystallinity of Ag NPs were confirmed by powder XRD analysis. The surface morphology and topography of Ag NPs were observed by TEM analysis. Size distribution and dispersion stability of Ag NPs was determined by DLS and Zeta potential analysis. The average particles size was 20.3 nm and zeta potential of -20.3 mV suggested its high dispersion stability. The characteristic functional groups of biomolecules capped on Ag NPs were identified by FT-IR analysis. Photocatalytic degradation activity showed that methylene blue was degraded 98.3% within 7 min, 97.34 % of rhodamine B within 9 min and 94.6% of methyl orange within 13 min by photocatalyst Ag NPs under UV light irradiation. Hence ECBP aqueous extract mediated Ag NPs could be used as the promising photocatalyst for the degradation of textile and paint industries effluents.

Keywords: Ag NPs, cotton ball peel, organic dyes, catalytic degradation of textile dyes, paint.

1. INTRODUCTION

Nanoparticles with unique and superior properties such as catalytic, magnetic, optical-electrical, and antibacterial over bulk materials have played as the most important and powerful tool for mankind. Synthesized noble metal nanoparticles (MNPs) with improved physicochemical properties [1, 2] have been used in various fields [3, 4] and among them silver nanoparticles (Ag NPs) has been used in interdisciplinary fields such as purification of water, environment pollutants dye degradation, medicine, biosensors, magnetic and electronics. In addition, Ag NPs shows toxicity towards a wide range of microorganisms and hence textiles, room sprays and food storage containers have used it extensively [5]. All physical and chemical methods such as chemical/electrochemical precipitation, laser pyrolysis, aerosol process, sol-gel process, mechanical milling, ball milling, thermal ablation, laser ablation and chemical reduction [6, 7, 8] have their own drawbacks. Physical methods are very expensive, time-consuming, need high energy and complicated instruments. On the other hand, chemical methods involve the use of harsh chemicals for the synthesis and resulted in the formation of unwanted by-products leading to the contamination of NPs [9]. Since Ag NPs

have been used in optical, electrical and human contacting application [10, 11, 12], it is necessary to move towards non-toxic cheap actions for green and safer Ag NPs fabrication. Biogenic synthesis of Ag NPs using bacteria [13] fungi [14, 15] enzymes [16] and plants [17-23] as reducing and stabilizing agents have been widely practiced from past decade as the best alternative to both chemical and physical conventional methods. Among these green reducing agents plant extracts has been executed widely to synthesize MNPs because other methods require the lengthy procedure of maintaining cell cultures and monitoring reactions [24, 25, 26]. Although a lot of works has been reported in this field, researchers are still working in this field to understand the potential of plant extracts as both reducing and stabilizing agent and also the chemistry involved in enhanced stability.

The present study reports (i) the synthesis of spherical Ag NPs by agro-waste empty cotton boll peels aqueous extract, (ii) characterization by using different instrumental techniques and (iii) catalytic efficiency for the degradation of organic pollutant dyes methylene blue, methyl orange and rhodamine B.

2. EXPERIMENTAL SECTION

Materials and methods.

Materials. Silver nitrate (AgNO_3), sodium borohydride (NaBH_4), rhodamine B (Rh-B), methylene blue (MB), methyl orange (MO) were purchased from Sigma-Aldrich, India. All other reagents used were of analytical grade. Empty cotton boll peels were collected from the cotton crop at Tungabhadra river area, Chilakaladona village, Mantralayam Mandal, Kurnool district of Andhra Pradesh, India. Distilled water was used throughout the study.

Preparation of the extract. The empty cotton boll peels (ECBP) were washed with tap water followed by distilled water. After washing ECBP was cut into small pieces and dried. The dried ECBP pieces were washed again with hot water to remove any soluble matter present and then dried overnight. The dried ECBP was powdered using a conventional grinder and sieved through 100 mesh sieve. 3 gm of sieved ECBP powder was added to 100 mL distilled water and heated in a water bath at 80°C for 30 min to prepare the aqueous extract. The extract was cooled at room

temperature, filtered through Whatman filter paper and then the freshly prepared ECBP aqueous extract was used for the synthesis of Ag NPs. pH of the aqueous extract was 3.5.

Synthesis of silver nanoparticles. 0.0339 gm of silver nitrate (AgNO_3 , 0.01 M) was dissolved in 20 mL double distilled water under stirring for 2 min at room temperature. 20 mL of freshly prepared aqueous ECBP extract was added drop by drop to AgNO_3 solution and stirred thoroughly at ambient condition (550 rpm, room temperature) for 30 min. The formation of Ag NPs was observed by the visual color change from light yellow to brown colour which confirmed the formation of Ag NPs. It was further confirmed by UV-Visible spectroscopy analysis.

Phytochemical screening of phytochemicals in ECBP extract. The aqueous extracts of ECBP was subjected to analysis of phytochemicals such as alkaloids, flavonoids, terpenoids, glycosides, steroids, tannins, carbohydrates, proteins and amino acids against the respective standards by the established methods described elsewhere [27]. **Table 1** shows the list of different category phytochemicals present in empty cotton boll peels aqueous extracts.

Table 1. Phytochemical test of Empty cotton boll peels aqueous extracts.

Test for	Test Name	Aqueous Extract
Phenol	Lead acetate test	+++
	Ferric chloride test	+++
Flavonoids	Alkaline Reagent test	+
Carbohydrates	Molish's test	++
	Benedict's test	++
Amino Acids	Ninhydrin test	+

+ = Present; ++ = Higher; +++ = Highest

GC-MS analysis of bioactive compounds. The GC-MS study identifies 13 phytochemicals which are present in methanol extract of the empty cotton boll peels. The identified compounds are DL-Alanine, N-acetyl (8.586 %), Trichloroacetamidoxime (21.034 %), 1-Chloro-but-1-en-3-yne (2.103 %), 4-(Hydroxy Methyl)-1-phenyl-2-azetidinone (0.926 %), Dodecane, 2,7,10-Trimethyl (1.229 %), 3-Cyano-3-Methyl-4-Oxopentanamide (5.378 %), Oxazole-4-Carboxylic acid, 2-Methyl (10.856 %), Oxalic acid, 6-Ethyl-oct-3-yl Isobutyl ester (13.200 %) and (+)-Trans-3,4-dimethyl-2-Phenyltetrahydro-1,4-Thiazine (11.669 %), Cyclobutane carboxamide, N-Tetrahydrofurfuryl (8.634 %), Sulphurous acid, Decyl 2-Propyl ester (5.766 %), 3,4-Dibromohex-3-ene-2,5-diol (4.067 %) and Silane, Dimethyl (Tetrahydrofurfuryloxy) Ethoxy (2.492 %) (**Table 2**). These identified bioactive compounds may act as reducing and stabilizing agent during the synthesis of Ag NPs.

Characterization of synthesized Ag NPs.

UV-Visible (UV-Vis) spectroscopy analysis. The initial characterization of the as-synthesized Ag NPs was carried out by

using UV-Visible spectroscopy (Jasco V-670 UV-Visible double beam spectrophotometer). UV-Vis spectrum was recorded within the wavelength range of 200-800 nm and the obtained data was plotted using Origin 8.0 software.

X-ray diffraction (XRD) analysis. The dried Ag NPs was used for XRD and FT-IR, DLS and TEM analysis. The XRD analysis of Ag NPs powder was carried out by using Bruker D8 diffractometer with $\text{Cu K}\alpha$ radiation ($\lambda=1.54^\circ$). The diffractogram was recorded in the scanning range (2θ value) of 10° to 90° with a scanning rate of $4^\circ/\text{min}$ and a step size of 0.02° .

Transmission electron microscopy (TEM) analysis

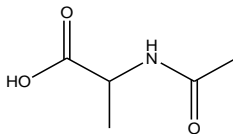
The size, shape and selected area electron diffraction (SAED) pattern of Ag NPs were analyzed by using high resolution transmission electron microscope (HR-TEM) (JEOL-JEM 2100 transmission electron microscope) with an acceleration voltage of 200 kV. 15 mg of powder Ag NPs was dispersed in 1mL of ethanol by sonication for 10 min using an ultrasonic bath. Ag NPs colloidal solution was placed on the carbon-coated grids and then the solvent was evaporated at ambient condition before analysis.

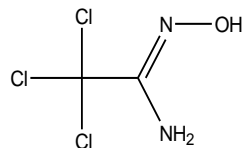
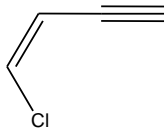
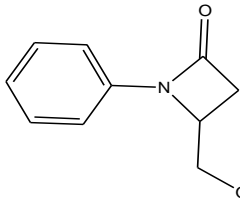
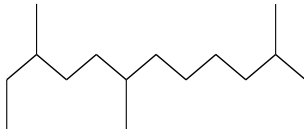
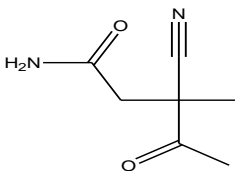
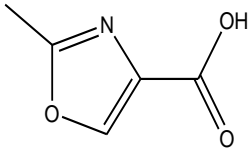
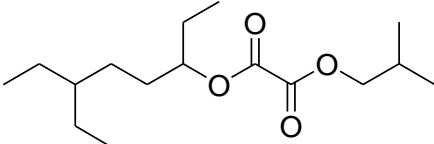
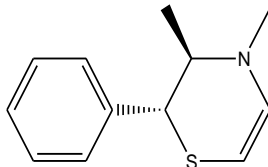
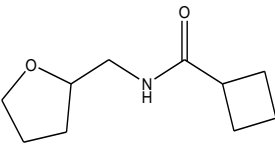
Dynamic light scattering (DLS) and Zeta potential analysis. Dynamic light scattering (DLS) technique was used to analyze average particles size of Ag NPs whereas measurement of polydispersity indexes (PDI) determined suspension stability. Zeta potential of Ag NPs dispersion was measured by Horiba scientific nanoparticci (nanoparticle analyzer, SZ-100) to judge the stability of NPs dispersion. The sample was interpreted in triplet at 20°C with a scattering angle of 173° . Zeta potential of the Ag NPs suspension was measured in cell culture medium at 25°C and 150 V in triplet for each sample using deionized water against calibration standards.

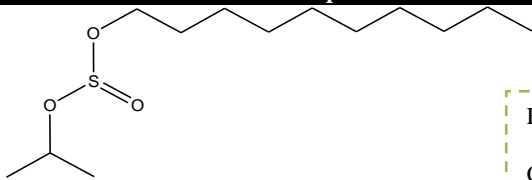
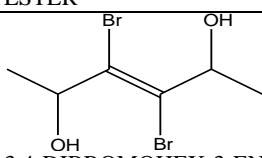
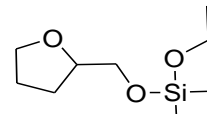
Fourier transform infrared (FTIR) analysis. The presence of functional groups on capped Ag NPs surface and residue of ECBP aqueous extract after solvent evaporation was identified by recording FTIR spectra of powder Ag NPs and ECBP powders using JASCO FT-IR 4100 (Shimadzu IR AFFINITY-1) in the diffuse reflectance mode at a resolution of 4 cm^{-1} via KBr pellets.

Catalytic activity of Ag NPs. The synthesized Ag NPs was checked for its catalytic activity towards degradation of different organic dyes such as rhodamine B (RhB), methylene blue (MB) and methyl orange (MO) at room temperature. Preliminary dye degradation was tested with NaBH_4 or with Ag NPs without NaBH_4 or with both of them at room temperature. Instantaneously intermediate forms of organic dyes were formed with NaBH_4 and remained as such for a long time. Specific doses of Ag NPs were added to the test solution to promote the catalytic degradation of dyes further and the progress of dye degradation was monitored using UV-Vis spectroscopy at regular time intervals.

Table 2. Phytochemical analysis of empty cotton boll peels aqueous extracts by GC-MS.

Entry	RT	Area %	Structure and Name of the compound
1	2.52	8.586	 <div style="display: flex; justify-content: space-between; align-items: center;"> <div>DL-ALANINE, N-ACETYL</div> <div style="border: 1px dashed green; padding: 5px;"> Formula $\text{C}_5\text{H}_9\text{O}_3\text{N}$ </div> </div>

Entry	RT	Area %	Structure and Name of the compound
2	2.73	21.034	 <div>Formula $C_2H_3ON_2Cl_3$</div> <p>TRICHLOROACETAMIDOXIME</p>
3	3.86	2.103	 <div>Formula C_4H_7Cl</div> <p>1-BUTEN-3-YNE, 1-CHLORO-, (Z)-</p>
4	12.86	0.926	 <div>Formula $C_{10}H_{11}O_2N$</div> <p>4-(HYDROXYMETHYL)-1-PHENYL-2-AZETIDINONE</p>
5	21.36	1.229	 <div>Formula $C_{15}H_{32}$</div> <p>DODECANE, 2,7,10-TRIMETHYL-</p>
6	21.97	5.378	 <div>Formula $C_7H_{10}O_2N_2$</div> <p>3-CYANO-3-METHYL-4-OXOPENTANAMIDE</p>
7	22.63	10.856	 <div>Formula $C_5H_5O_3N$</div> <p>OXAZOLE-4-CARBOXYLIC ACID, 2-METHYL</p>
8	23.35	13.200	 <div>$C_{16}H_{30}O_4$</div> <p>OXALIC ACID, 6-ETHYLOCT-3-YL ISOBUTYL ESTER</p>
9	24.17	11.669	 <div>Formula $C_{12}H_{17}NS$</div> <p>(+)-TRANS-3,4-DIMETHYL-2-PHENYLTETRAHYDRO-1,4-THIAZINE</p>
10	24.87	8.634	 <div>Formula $C_{10}H_{17}O_2N$</div> <p>CYCLOBUTANECARBOXAMIDE, N-TETRAHYDROFURFURYL-</p>

Entry	RT	Area %	Structure and Name of the compound
11	25.16	5.766	 <div>Formula $C_{13}H_{28}O_3S$</div> <p>SULFUROUS ACID, DECYL 2-PROPYL ESTER</p>
12	26.31	4.067	 <div>Formula $C_6H_{10}O_2Br_2$</div> <p>3,4-DIBROMOHEX-3-ENE-2,5-DIOL</p>
13	27.02	2.492	 <div>Formula $C_9H_{20}O_3Si$</div> <p>SILANE, DIMETHYL(TETRAHYDROFURFURYLOXY)ETHOXY-</p>

3. RESULTS SECTION

Formation of Ag NPs was observed by the visual colour change which was confirmed by UV-visible spectroscopy. The reduction of Ag^+ ion to Ag^0 NPs was instantaneous i.e. an immediate colour change occurred within a short period of time from light yellow to a brown colour indicating the formation of Ag NPs in the presence of ECBP extract. This colour change was due to surface Plasmon resonance (SPR) excitation [28]. Figure 1A displays the UV-vis absorption spectra of Ag NPs with a distinct characteristic maximum absorption peak at 432 nm by recording the spectra of the colloidal solution between 200-800 nm. The similar result was observed at 410-414 nm for Ag NPs by Zielinska et al [29]. As spherical Ag NPs exhibit a single Plasmonic band at 432 nm the synthesized Ag NPs were isotropic spherical in shape [30]. Also, the aqueous dispersion of these particles was very clear and stable for 60 days (Fig. 1B) without aggregation of particles.

Morphology i.e. size and shape of the synthesized Ag NPs was determined by TEM analysis (Fig. 2A-C). TEM images confirmed spherical shaped Ag NPs which is in clear agreement with UV-visible finding and the average size of particles is 12 nm. Fig. 2A-C shows the thin layer of capping on Ag NPs surface which is responsible for the smaller size and higher stability of the synthesized Ag NPs. The crystalline nature of Ag NPs was further confirmed by SAED pattern (Fig. 2D) which represents the diffraction rings with bright spots indexed to the (111), (200), (142), (220) and (311) crystal planes of the face-centered cubic structure. Fig. 2E shows the particles size distribution of the synthesized Ag NPs with a size range of 5-30 nm. The EDAX pattern confirmed the chemical composition of Ag NPs (elemental weight percentage 84.28%, atomic weight percentage 42.03%) and oxygen (elemental weight percentage 11.13%, atomic weight percentage 37.43%) without other elements indicating the purity of the synthesized Ag NPs (Fig. 2F).

The XRD pattern of synthesized Ag NPs (Fig. 3) displays five dissimilar peaks at 2θ values of 38.33, 44.08, 54.36, 64.46 and 77.52 which correspond to the (111), (200), (142), (220) and

(311) inter-planar reflections of the cubic crystal system with lattice parameter 'a' of 4.0860 Å. The lattice plane with hkl value of "111" has more intensity because of its predominant orientation than other peaks [31]. The enlargement of the Bragg's peaks indicates the formation of small crystallite size. These results perfectly agreed with *Calendula officinalis*-plant based synthesized Ag NPs [32]. The obtained XRD pattern was compared with JCPDS data card (JCPDS NO: 96-901-3046) which confirms the crystalline nature of the synthesized Ag NPs. The average crystallite or grain size was calculated by using Scherrer equation as $D = K\lambda/\beta\cos(\theta)$, where D is the average crystal size, λ is the X-ray wavelength ($\lambda = 1.5406$ Å), K is the Scherrer coefficient (0.891), β is the full width at half maximum intensity (FWHM) in radians and θ is Bragg's angle in degree (2θ). The average crystallite size was found to be 13 nm. DLS study results reveal the size distribution of the synthesized Ag NPs (Fig. 4). The average particles diameter of the synthesized Ag NPs was 20.3 nm (Fig. 4b) and also zeta potential of the synthesized Ag NPs suspension was -27.3 mV which confirms its stability in aqueous solution (Fig. 4a). A similar result was observed for synthesized Ag NPs by *Uratica dioica* leaf extracts [33].

FTIR spectrum of residue sample of ECBP aqueous extract after solvent evaporation reveals the presence of functional groups responsible for the synthesis of Ag NPs. FTIR analysis was carried out for the residue before reduction and Ag NPs. Fig. 5B shows the FTIR spectrum of residue and the peak appeared at 3346.50 cm^{-1} which corresponds to O—H stretching vibration. The strong band appeared at 3257.77 cm^{-1} could be due to —N—H stretching vibration, band at 1737.86 cm^{-1} due to carbonyl (C=O) stretching vibration, the strong broad located at 1606.70 cm^{-1} due to carbon and nitrogen for amine (C—N) bending vibration, the weak band at 1392.61 cm^{-1} due to nitrogen and oxygen (N—O) stretching vibration, the band at 1105.21 cm^{-1} due to carbon and oxygen (C—O) stretching vibration for carboxylic acid or alcohols or esters. Fig. 5A shows FTIR spectrum of Ag NPs powder which indicates the participation of alkaloids, flavonoids and phenols,

proteins and poly-phenols having functional groups of carboxylic acid, ketones, amines alcohol in the bio-reduction. FTIR spectrum of Ag NPs shows a peak at 3346.50 to 3359.88 cm^{-1} which correspond to hydroxyl ($-\text{OH}$) stretching vibration due to the capping of bio-molecules on the surface of Ag NPs. Also, peak intensity for amine, carbonyl groups slightly increases the stretching vibration. The peak at 2336.98 cm^{-1} is assigned to nitrile ($-\text{C}\equiv\text{N}$) stretching vibration.

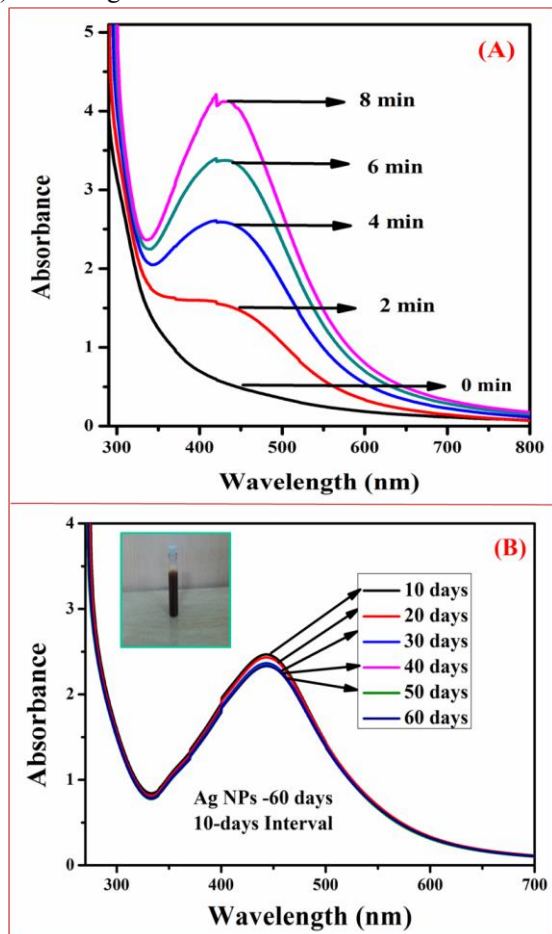


Figure 1. UV-Visible spectra: Progress of Ag NPs formation with time in min (A) and stability of Ag NPs suspension with time in days (B).

The above mentioned vibration peaks associated with the organic molecules in plant extracts like proteins, carbohydrates, alkaloids, flavonoids and terpenoids are reported by other researchers also [49, 50]. The presence of different functional groups on the surface of Ag NPs indicates capping of biomolecules and their involvement in the stabilization of Ag NPs. The changes in peak positions in FTIR spectrum of Ag NPs indicate the participation of biomolecules such as alkaloids, flavonoids and phenols, proteins and polyphenols having functional groups of carboxylic acid, ketones, amines and alcohol during reduction.

Catalytic activity of Ag NPs. The organic dyes such as MB, RhB and MO are common organic pollutants in industrial and agriculture wastewater [34]. Water pollution due to effluents from textile dyeing industry causes a serious environmental problem because these dyes undergo chemical changes under environmental conditions to more toxic compounds. Only NaBH_4 did not degrade pollutant dyes without a catalyst, but degradation was carried out in the presence of both NaBH_4 and nanocatalyst Ag NPs due to the high surface area of nanoparticles in the present

study. A similar report is available in literature where degradation of organic dyes was carried out by sodium borohydride with *Trigonella foenum-graecum* seeds extract mediated synthesized Ag NPs as catalyst [35]. Also, several published literatures reported catalytic dye degradation by different nanomaterials [36-48].

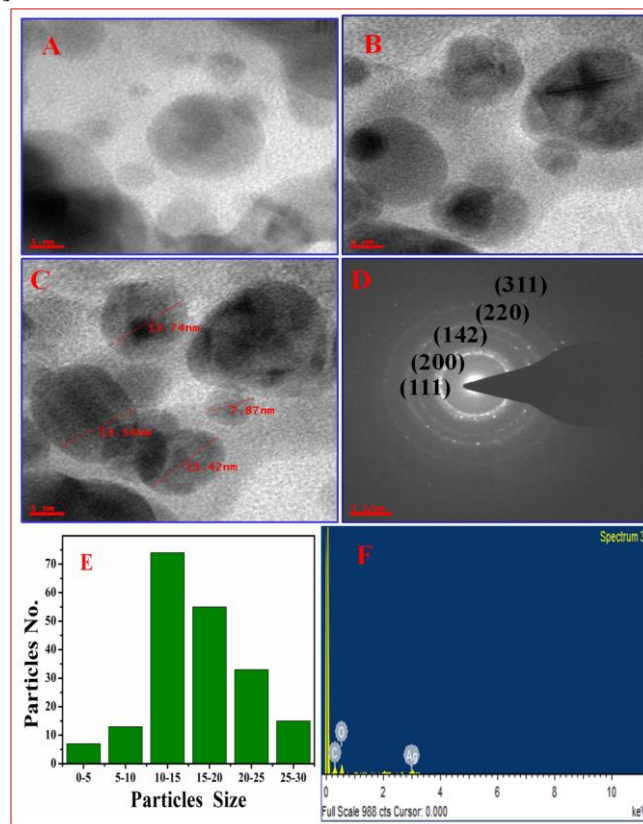


Figure 2. TEM images of synthesized Ag NPs (A, B and C), SAED pattern (D), Particles size distribution (E) and EDAX pattern (F).

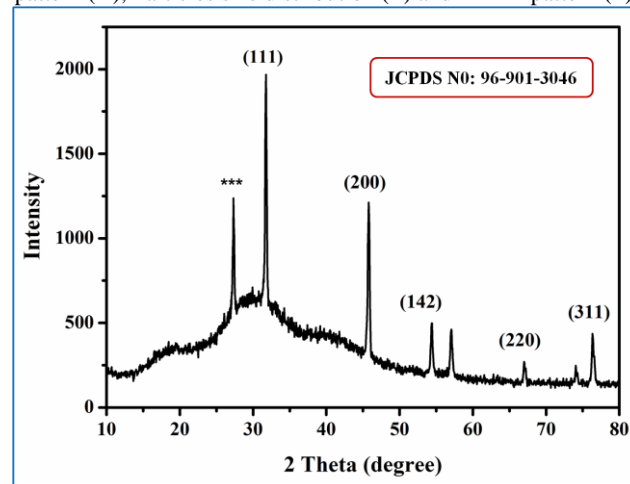


Figure 3. X-ray diffraction pattern of synthesized Ag NPs.

Degradation study of Methylene Blue (MB) by Ag NPs catalyst. Methylene blue, known as methylthionium chloride, a heterocyclic aromatic dye is used exclusively in the textile industry for years. UV-visible spectra of MB dye show a strong absorption band at 665 nm corresponding to $n-\pi^*$ transition. The progress of degradation process of a sample solution [$3 \text{ mL } 1 \times 10^{-4} \text{ M MB}$, $200 \mu\text{L } 0.05 \text{ M NaBH}_4$ and finally $150 \mu\text{L Ag NPs}$ (1 mg mL^{-1})] was monitored by UV-vis spectrophotometer at 665 nm and MB dye degraded within 7 min (Fig. 6A) [51-53]. Fig. 6B shows the degradation progress of MB dye under the same condition without a catalyst, but up to 40 min there was no change in colour i.e. no degradation of the dye solution was observed. As

the primary concentration of NaBH_4 was in excess and its concentration was considered as stable all over the reaction, the degradation rate was independent of NaBH_4 concentration and followed pseudo-first order kinetics (Fig. 6C) [54]. The rate constant k was calculated as 0.04627 min^{-1} . Fig. 6D show the degradation kinetics of MB dye and photocatalytic degradation efficiency (%) is calculated by using the formula as “Degradation (%) = $[(A_0 - A_t) \times 100 / A_0]$ ”, where A_0 is the initial dye absorbance without irradiation, A_t is absorbance value at time “t”. It is clear that MB dye degraded 98.3% within 7 min.

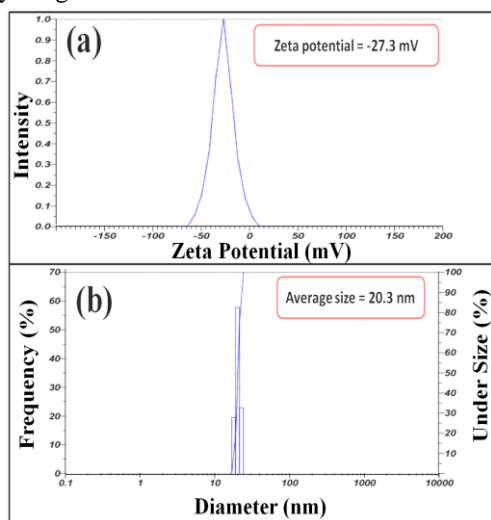


Figure 4. DLS study for Zeta potential determination of synthesized Ag NPs suspension (a) and average Ag NPs size distribution (b).

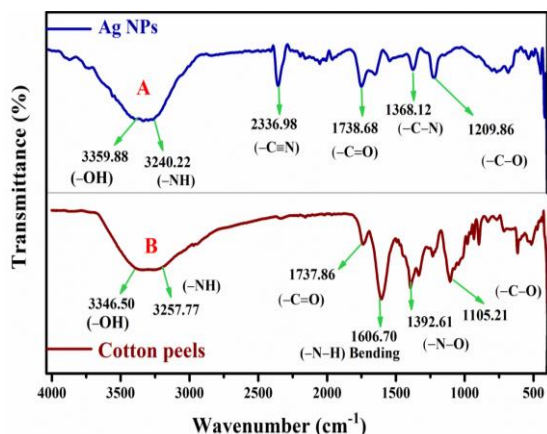


Figure 5. FTIR spectra of synthesized Ag NPs (A) and residue of cotton peels aqueous extract after solvent evaporation (B).

Degradation study of Rhodamine B (RhB) by Ag NPs catalyst. Rhodamine B (RhB) is an aromatic/fluorescent dye which belongs to xanthene family. It is widely used in the textile industry. Degradation progress of RhB dye solution (3 mL , $1 \times 10^{-4} \text{ M}$) with relay electron donor NaBH_4 ($200 \mu\text{L}$ 0.05 M) and catalyst Ag NPs [$150 \mu\text{L}$ Ag NPs (1 mg mL^{-1})] was monitored by UV-Vis spectrophotometer at 549 nm (Fig. 7A). As the redox potential between dye and sodium borohydride is huge, Ag NPs diminished the activation energy barrier by forming an intermediate compound which promoted degradation of dye molecules rapidly. As NaBH_4 alone did not degrade RhB dye up to 40 min (Fig. 7B), but the catalytic amount of Ag NPs with NaBH_4 resulted in a red coloured aqueous solution of RhB which exhibited a strong absorption band in the range from $200\text{--}800 \text{ nm}$ within 9 min . Similarly we noticed RhB dye degradation in the presence of Ag@Cu and Ag@TiO₂ bimetallic NPs [55,56]. The reduction kinetics of RhB was a pseudo-first order reaction (Fig. 7C) and the

rate constant k was 0.2158 min^{-1} [57]. Fig. 7D shows the percentage of RhB dye degradation and the total degradation efficiency was calculated by using the following equation as “ $\ln(C_t/C_0) = -kt$ ”, where C_0 is the initial concentration of RhB before irradiation, C_t is the time when the sample was taken for absorbance measurement after irradiation. Fig. 7D shows the degradation efficiency of RhB (97.34%) within 9 min at 549 nm .

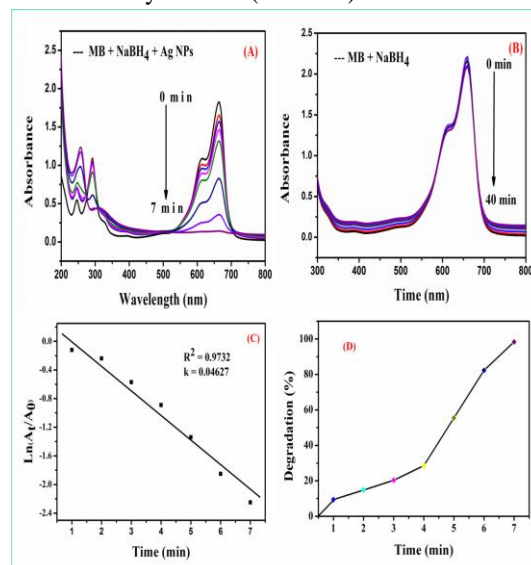


Figure 6. UV-Visible spectra for the degradation of MB dye by NaBH_4 in the presence of catalyst Ag NPs (A), without catalyst Ag NPs (B,) degradation kinetics of MB dye (C) & degradation of MB dye (%) with time in min (D).

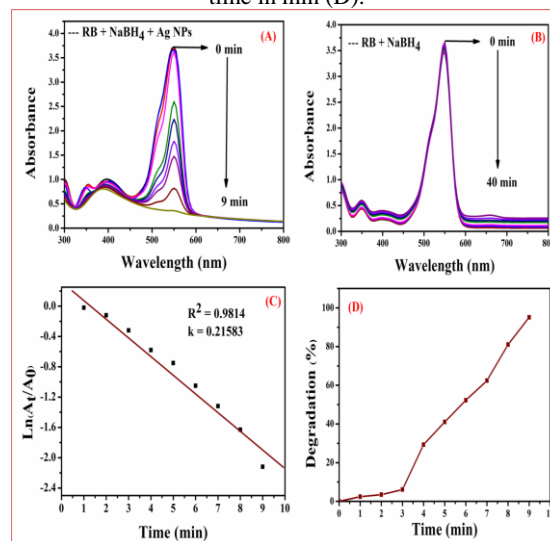


Figure 7. UV-Visible spectra for the degradation of RhB dye by NaBH_4 in the presence of catalyst Ag NPs (A), without catalyst Ag NPs (B,) degradation kinetics of RhB dye (C) & degradation of RhB dye (%) with time in min (D).

Degradation study of Methyl Orange (MO) by Ag NPs catalyst. Fig. 8A shows the degradation of MO dye by catalyst Ag NPs with NaBH_4 which was monitored by UV-Visible spectrophotometer at a λ_{max} of 463 nm . Degradation progress of MO dye solution ($1 \times 10^{-4} \text{ M}$ MO, 3 mL) was monitored in the presence of $200 \mu\text{L}$ NaBH_4 (0.05 M) with or without Ag NPs ($150 \mu\text{L}$ 1 mg mL^{-1} Ag NPs) and the dye colour rapidly disappeared within 13 min at 463 nm whereas there was no change in absorbance peak intensity of UV-Visible spectra monitored at 463 nm up to 40 min without catalyst Ag NPs which suggests no degradation without catalyst (Fig. 8B). In addition, the kinetics of dye degradation was evaluated by using the formula “ $\ln(C_t/C_0) = -kt$ ”, where C_0 is a concentration of MO dye at time $t = 0$, C_t is the

concentration at time t , and k is rate constant. It followed pseudo first order kinetics and the rate constant k was 0.04627 min^{-1} (Fig. 8C). Figure 8D shows the percentage of MO dye degradation with time and the total degradation efficiency was calculated by using the following equation as "[Degradation (%) = $(A_0 - A_t) \times 100 / A_0$]. It was 94.6% within 13 min in the presence of both electron donor NaBH_4 and catalyst Ag NPs [58, 59].

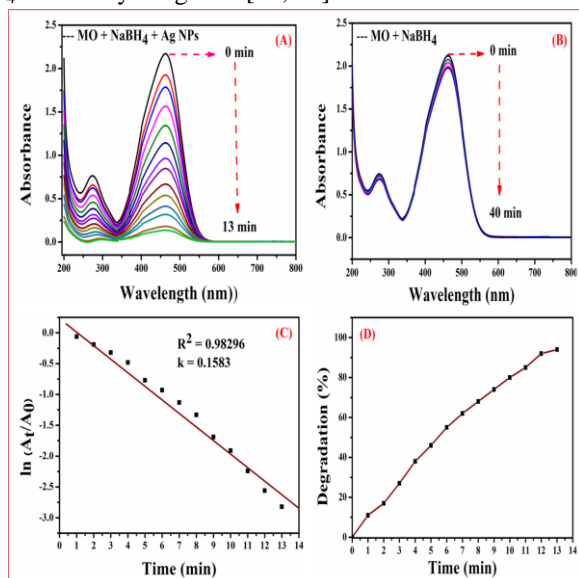


Figure 8. UV-Visible spectra for the degradation of MO dye by NaBH_4 in the presence of catalyst Ag NPs (A), without catalyst Ag NPs (B), degradation kinetics of MO dye (C) & degradation of MO dye (%) with time in min (D).

Information on the degradation of MB, MO and RhB is summarized by considering the ratio of Ag NPs catalyst dose to dye conc. ($\mu\text{g}/\mu\text{g}$), size and shape of NPs and degradation time (min) in the presence of NaBH_4 [36-47] (Table 3). Also, information on Au NPs catalysed the degradation of Congo red and rhodamine B [41, 42, 43] is summarized in Table 3 for comparison. It is clearly evident that the degradation time solely depends on the ratio of Ag NPs catalyst dose to dye conc. ($\mu\text{g}/\mu\text{g}$), size and shape of nanoparticles (Table 3). Results of earlier reports on the reduction of MB to leuco MB [36, 38, 40] as well as RhB dye reduction [42, 43] support our observation. Also, earlier

reports show that the reduction of MO happened by the electron transfer from donor to acceptor via nano-catalyst [44, 45, 47]. Hence the synthesized Ag NPs catalyst exhibited enhanced activity compared to others (Table 3) which may be due to smaller particles size with the uniform spherical shape. The degradation study results show that MB degraded within 7 min with a rate constant of 0.04627 min^{-1} , RhB degraded within 9 min with a rate constant of 0.21583 min^{-1} while MO degraded within 13 min with a rate constant of 0.15832 min^{-1} which suggests different response of individual dye under an identical dose of Ag NPs in the presence of NaBH_4 . Actually metallic nanoparticles served as electron relays in a redox reaction whereas MB, RhB and MO behaved as electrophile and BH_4^- as a nucleophile with respect to NPs (Fig. 9) [60]. The nucleophile NaBH_4 donated an electron to Ag NPs and electrophiles i.e. dyes captured electrons via Ag NPs for degradation to CO_2 and H_2O [61]. Consequently, the synthesized Ag NPs exhibited good catalytic performance by reducing activity energy of the dye-Ag NPs adducts and could be utilized as a promising catalyst in degrading toxic and hazardous organic pollutants dyes from industrial effluents and wastewater.

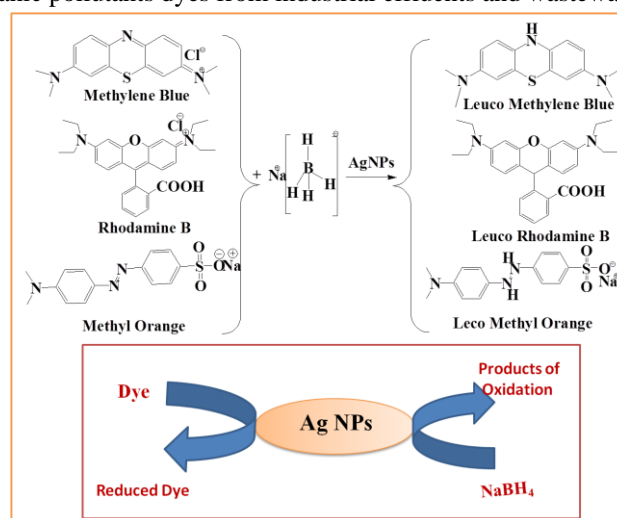


Figure 9. Degradation mechanism of MB, RhB and MO dyes by NaBH_4 in the presence of catalyst Ag NPs.

Table 3. Catalytic activity of Ag NPs from different literature reports.

NPs	Dye solution	Con. NPs/dye (mg/mg)	Size/shape	Time	Ref
Ag NPs	Methylene blue	85.6032	17-66 nm/ spherical	30 min	[36]
Ag NPs	Congo red	13.5421	30-200 nm/ spherical	240 min	[37]
Ag NPs	Methylene blue	6.0512	20 nm/ spherical	10 min	[38]
Ag NPs	Direct Orange	0.6667	54.8 nm/spherical	18 min	[39]
Ag NPs	Methylene blue	0.4801	28 nm/ spherical	20 min	[40]
Ag NPs	Methylene blue	1.5632	12 nm/ spherical	7 min	Present work
^L Au NPs	Congo red	9.8684	2.67 nm/spherical	10 min	[41]
*Au NPs	Rhodamine B	4.2194	4 nm/ spherical	10 min	[42]
Ag NPs	Rhodamine B	2.3951	51.32/spherical	9 min	[43]
Ag NPs	Rhodamine B	1.0438	12 nm/ spherical	9 min	Present work
Ag/TiO ₂	Methyl Orange	20.3668	24 nm/spherical	9 min	[44]
Ag NPs	Methyl Orange	1.4548	23-25 nm/spherical	60 min	[45]
Ag NPs	Congo red	1.1962	20-120 nm/spherical	45 min	[46]
Ag NPs	Methyl Orange	0.8000	11-12 nm/spherical	20 min	[47]
Ag NPs	Methyl Orange	1.5275	12 nm/spherical	13 min	Present work

L = (@Tan-ESM), * = (Supported CeO₂-TiO₂)

4. CONCLUSIONS

In the present study, Ag NPs was synthesized in an efficient and cost-effective manner via green method by using

empty cotton boll peels aqueous extract at room temperature. The synthesized Ag NPs showed good stability for at least two months

which was supported with high zeta-potential value. TEM analysis revealed the mean diameter of the synthesized Ag NPs as 12 nm with spherical morphology and reasonably monodispersed. Ag NPs served as an efficient catalyst for the reduction of organic pollutants such as MB, MO and RhB dyes in the presence of NaBH₄. The significant catalytic performances of Ag NPs were

due to their high surface to volume ratio providing more active sites for interaction to dye molecules and reduced the degradation time by reducing activation energy. The results of this study suggest that the synthesized Ag NPs could be used effectively in degrading toxic organic pollutant dyes from industrial effluents and wastewater.

5. REFERENCES

- [1] Mittal A.K., Chisti Y., Banerjee U.C., Synthesis of metallic nanoparticles using plant extracts, *Biotechnol. Adv.*, 31, 346-356, **2013**.
- [2] Rao V.K., Ghildiyal P., Radhakrishnan T.P., In situ fabricated Cu-Ag nanoparticle-embedded polymer thin film as an efficient broad spectrum SERS substrate, *J. Phys. Chem. C. A.*, 12, 1339-1348, **2013**.
- [3] Zeng H., Sun S., Syntheses, properties, and potential applications of multicomponent magnetic nanoparticles, *Adv. Funt. Mater.*, 18, 391-400, **2008**.
- [4] Sreekanth T.V.M., Ravikumar S., Eom I.Y., Green synthesized silver nanoparticles using Nelumbo nucifera root extract for efficient protein binding, antioxidant and cytotoxicity activities, *J. Photochem. Photobiol.*, 141, 100-105, **2014**.
- [5] Maddinedi S.B., Mandal B.K., Ranjan S., Dasgupta N., Diastase assisted green synthesis of size-controllable gold nanoparticles Title, *RSC Adv.*, 5, 26727-26733, **2015**.
- [6] Kim Y.S., Kim K.K., Shin S.M., Park S.M., Hah S.S., Cytotoxicity of ultra-pure TiO₂ and ZnO nanoparticles generated by laser ablation Title, *Bull. Korean Chem. Soc.*, 33, 3265, **2012**.
- [7] Poddar P., Gass J., Rebar D., Srinath S., Srikanth H., Morrison S., Carpenter E.E., Magnetocaloric effect in ferrite nanoparticles Title, *J. Magn. Magn. Mater.*, 307, 227-231, 2006.
- [8] Reisfeld R., Grinberg M., Levchenko V., Kuklinski B., Mahlik S., Magdassi S., Grouchko M., Sol-gel glasses with enhanced luminescence of laser dye Rhodamine B due to plasmonic coupling by copper nanoparticles Title, *Opt. Mater.*, 36, 1611-1615, **2014**.
- [9] Ajitha B., Reddy Y.A.K., Shameer S., Rajesh K., Suneetha Y., Reddy P.S., Lantana camara leaf extract mediated silver nanoparticles: antibacterial, green catalyst Title, *J. Photochem. Photobiol.*, 149, 84-92, **2015**.
- [10] Roopan S.M., Surendra T.V., Elango G., Kumar S.H.S., Biosynthetic trends and future aspects of bimetallic nanoparticles and its medicinal applications Title, *Appl. Microbiol. Biotechnol.*, 98, 5289-5300, **2014**.
- [11] Anand K.K.H., Mandal B.K., Activity study of biogenic spherical silver nanoparticles towards microbes and oxidants Title, *Spectrochim. Acta A.*, 135, 639-645, 2015.
- [12] Safdar M., Junejo Y., Balouch A., Safdar M., Junejo Y., Balouch A., Efficient degradation of organic dyes by heterogeneous cefdinir derived silver nanocatalyst Title, *Ind. Eng. Chem. Res.*, 31, 216-222, **2015**.
- [13] Malarkodi C., Rajeshkumar S., Paulkumar K., Gnanajobitha G., Vanaja M., Annadurai G., Bacterial synthesis of silver nanoparticles by using optimized biomass growth of Bacillus sp Title, *Nanosci. Nanotechnol.*, 3, 26-32, **2013**.
- [14] Vahabi K., Mansoori G.A., Karimi S., Biosynthesis of silver nanoparticles by fungus Trichoderma reesei (a route for large-scale production of AgNPs) Title, *Inscience J.*, 1, 65-78, **2011**.
- [15] Moghaddam A.B., Namvar F., Moniri M., Tahir P.M., Azizi S., Mohamad R., Nanoparticles biosynthesized by fungi and yeast: a review of their preparation, properties, and medical applications Title, *Molecules*, 20, 16540-16565, **2015**.
- [16] Sanghi R., Verma P., Puri S., Enzymatic formation of gold nanoparticles using Phanerochaete chrysosporium Title, *Adv. Chem. Eng. Sci.*, 1, 154-162, **2011**.
- [17] Irvani S., Green synthesis of metal nanoparticles using plants Title, *Green Chemistry*, 13, 2638-2650, **2011**.
- [18] Kumar R., Roopan S.M., Prabhakarn A., Khanna V.G., Chakroborty S., Agricultural waste Annona squamosa peel extract: biosynthesis of silver nanoparticles Title, *Spectrochim. Acta A.*, 90, 173-176, **2012**.
- [19] Ahmed S., Ahmad M., Swami B.L., Ikram S., A review on plants extract mediated synthesis of silver nanoparticles for antimicrobial applications: a green expertise Title, *J. Adv. Res.*, 7, 17-28, **2016**.
- [20] Gopinath M., Subbaiya R., Selvam M.M., Suresh D., Synthesis of copper nanoparticles from Nerium oleander leaf aqueous extract and its antibacterial activity Title, *Int. J. Curd. Microbiol. App., Sci.*, 3, 814-818, **2014**.
- [21] Kumar D.A., Palanichamy V., Roopan S.M., Photocatalytic action of AgCl nanoparticles and its antibacterial activity Title, *J. Photochem. Photobiol.*, 138, 302-306, **2014**.
- [22] Chen H., Wang J., Huang D., Chen X., Zhu J., Sun D., Huang J., Li Q., Plant-mediated synthesis of size-controllable Ni nanoparticles with alfalfa extract Title, *Mater. Lett.*, 122, 166-169, **2014**.
- [23] Aromal S.A., Philip D., Green synthesis of gold nanoparticles using Trigonella foenum-graecum and its size-dependent catalytic activity Title, *Spectrochim. Acta A.*, 97, 1-5, 2012.
- [24] Ahmed K.B.A., Senthilnathan R., Megarajan S., Anbazhagan V., Sunlight mediated synthesis of silver nanoparticles using redox phytoprotein and their application in catalysis and colorimetric mercury sensing Title, *J. Photochem. Photobiol.*, 151, 39-45, **2015**.
- [25] Awwad A.M., Salem N.M., Green Synthesis of Silver Nanoparticles by Mulberry Leaves Extract Title, *J. Nanosci. Nanotechnol.*, 2, 125-128, **2012**.
- [26] Lakshminpathy R., Reddy B.P., Sarada N., Chidambaram K., Pasha S.K., Watermelon rind-mediated green synthesis of noble palladium nanoparticles: catalytic application Title, *Appl. Nanosci.*, 5, 223-228, **2015**.
- [27] Tiwari P., Kumar B., Kaur M., Kaur G., Kaur H., Phytochemical screening and extraction: a review Title, *Int. Pharm. Sci.*, 1, 98-106, **2011**.
- [28] Joseph S., Mathew B., Microwave-assisted green synthesis of silver nanoparticles and the study on catalytic activity in the degradation of dyes Title, *J. Mol. Liq.*, 204, 184-191, **2015**.
- [29] Zielińska A., Skwarek E., Zaleska A., Gazda M., Hupka J., Preparation of silver nanoparticles with controlled particle size Title, *Procedia Chem.*, 1, 1560-1566, **2009**.
- [30] Reddy B.N.K., Kumar H.A.K., Mandal B.K., Biofabricated silver nanoparticles as green catalyst in the degradation of different textile dyes Title, *J. Environ. Chem. Eng.*, 4, 56-64, **2016**.
- [31] Edison T.J.I., Sethuraman M., Instant green synthesis of silver nanoparticles using Terminalia chebula fruit extract and evaluation of their catalytic activity on reduction of methylene blue Title, *Process Biochem.*, 47, 1351-1357, **2012**.
- [32] Baghizadeh A., Ranjbar S., Gupta V.K., Asif M., Pourseyedi S., Karimi M.J., Mohammadinejad R., Green synthesis of silver nanoparticles using seed extract of Calendula officinalis in liquid phase Title, *J. Mol. Liq.*, 207, 159-163, **2015**.
- [33] Kumari J., Baunthiyal M., Singh A., Characterization of silver nanoparticles synthesized using Urtica dioica Linn. leaves and their synergistic effects with antibiotics Title, *J. Radiat. Res. Appl. Sci.*, 9, 217-227, **2016**.
- [34] Devi H.S., Singh N.R., Singh H.P., Singh T.D., Facile synthesis of biogenic gold nanocatalyst for efficient degradation of organic pollutants Title, *J. Environ. Chem Eng.*, 3, 2042-2049, **2015**.
- [35] Vidhu V., Philip D., Catalytic degradation of organic dyes using biosynthesized silver nanoparticles Title, *Micron.*, 56, 54-62, **2014**.
- [36] Sreekanth T.V.M., Jung M., Eom I., Green synthesis of silver nanoparticles, decorated on graphene oxide nanosheets and their catalytic activity Title, *Appl. Sci. Res.*, 361, 102-106, **2016**.
- [37] Saravanan C., Rajesh R., Kaviarasan T., Muthukumar K., Kavitate D., Shetty P.H., Synthesis of silver nanoparticles using bacterial exopolysaccharide and its application for degradation of azo-dyes Title, *Biotechnol. Rep.*, 15, 33-40, **2017**.
- [38] Khodadadi B., Bordbar M., Nasrollahzadeh M., Achillea millefolium L. extract mediated green synthesis of waste peach kernel shell supported silver nanoparticles: Application of the nanoparticles for catalytic reduction of a variety of dyes in water Title, *J. Colloids Interface Sci.*, 493, 85-93, **2017**.

[39] Yao P., Zhang J., Xing T., Chen G., Tao R., Choo K., Green synthesis of silver nanoparticles using grape seed extract and their application for reductive catalysis of Direct Orange 26 Title, *Ind. Eng. Chem. Res.*, 58, 74-79, **2018**.

[40] Hamed S., Shojasadati S.A., Mohammadi A., Evaluation of the catalytic, antibacterial and anti-biofilm activities of the *Convolvulus arvensis* extract functionalized silver nanoparticles Title, *J. Photochem. Photobiol.*, 167, 36-44, **2017**.

[41] Liu X., Liang M., Liu M., Su R., Wang M., Qi W., He Z., Highly efficient catalysis of azo dyes using recyclable silver nanoparticles immobilized on tannic acid-grafted eggshell membrane Title, *Nanoscale Res. Lett.*, 11, 440, **2016**.

[42] Saikia P., Miah A.B.U.T., Das P.P., Highly efficient catalytic reductive degradation of various organic dyes by Au/CeO₂-TiO₂ nano-hybrid Title, *J. Chem. Sci.*, 129, 81-93, 2017.

[43] Francis S., Joseph S., Koshy E.P., Mathew B., Green synthesis and characterization of gold and silver nanoparticles using *Mussaenda glabrata* leaf extract and their environmental applications to dye degradation Title, *Mater. Sci. Eng. B.*, 24, 17347-17357, **2017**.

[44] Atarod M., Nasrollahzadeh M., Sajadi S.M., *Euphorbia heterophylla* leaf extract mediated green synthesis of Ag/TiO₂ nanocomposite and investigation of its excellent catalytic activity for reduction of variety of dyes in water Title, *J. Colloids Interface Sci.*, 462, 272-279, **2016**.

[45] Eman A., Eco-friendly production of silver nanoparticles from peel of tangerine for degradation of dye Title, *World J. Nano Sci. Eng.*, 5, 10-16, **2015**.

[46] Anand K., Kaviyarasu K., Muniyasamy S., Roopan S.M., Gengan R.M., Chuturgoon A.A., Bio-synthesis of silver nanoparticles using agroforestry residue and their catalytic degradation for sustainable waste management Title, *J. Cluster Sci.*, 28, 2279-2291, **2017**.

[47] Shadakshari S., Santhosh A.S., Swamy N.K., Suresh G.S., Melo J.S., Mallu P., Biosynthesis of silver nanoparticles using *Convolvulus pluricaulis* leaf extract and assessment of their catalytic, electrocatalytic and phenol remediation properties Title, *Adv. Mater. Lett.*, 7, 383-389, **2016**.

[48] Suvith V.S., Philip D., Catalytic degradation of methylene blue using biosynthesized gold and silver nanoparticles Title, *Spectrochim. Acta A.*, 118, 526-532, **2014**.

[49] Kumar K.P., Paul W., Sharma C.P., Green synthesis of silver nanoparticles with *Zingiber officinale* extract and study of its blood compatibility Title, *Bio Nano Sci.*, 2, 144-152, **2012**.

[50] Raja S., Ramesh V., Thivaharan V., Antibacterial and anticoagulant activity of silver nanoparticles synthesised from a novel source—pods of *Peltophorum pterocarpum* Title, *Ind. Eng. Chem. Res.*, 29, 257-264, **2015**.

[51] Maddinedi S.B., Mandal B.K., Maddili S.K., Biofabrication of size controllable silver nanoparticles—a green approach, *J. Photochem. Photobiol.*, 167, 236-41, **2017**.

[52] Veisi H., Azizi S., Mohammadi P., Green synthesis of the silver nanoparticles mediated by *Thymbra spicata* extract and its application as a heterogeneous and recyclable nanocatalyst for catalytic reduction of a variety of dyes in water, *J. Clean Prod.*, 170, 1536-43, **2018**.

[53] Jha M., Shimpi N.G., Spherical nanosilver: Bio-inspired green synthesis, characterizations, and catalytic applications, *Nano-Structures & Nano-Objects*, 16, 234-49, **2018**.

[54] Jishma P., Narayanan R., Snigdha S., Thomas R., Radhakrishnan E.K., Rapid degradative effect of microbially synthesized silver nanoparticles on textile dye in presence of sunlight, *Biocatal. Agric. Biotechnol.*, 14, 410-7, **2018**.

[55] Khan Z., Bashir O., Khan MN, Khan TA, Al-Thabaiti SA. Cationic surfactant assisted morphology of Ag@ Cu, and their catalytic reductive degradation of Rhodamine B, *J. Mol. Liq.*, 248, 1096-108, **2017**.

[56] Liang H., Jia Z., Zhang H., Wang X., Wang J., Photocatalysis oxidation activity regulation of Ag/TiO₂ composites evaluated by the selective oxidation of Rhodamine B, *Appl. Surf. Sci.*, 422, 1-0, **2017**.

[57] Reddy Bogireddy N.K., Anand K.K., Mandal B.K., Catalytic efficiency of green synthesized palladium nanoparticles by *Sterculia acuminata* extract towards abatement of organic pollutants, *Biointerface Res. Appl. Chem.*, 8(3), 3319-23, **2018**.

[58] Khodadadi B., Bordbar M., Yeganeh-Faal A., Nasrollahzadeh M., Green synthesis of Ag nanoparticles/clinoptilolite using *Vaccinium macrocarpon* fruit extract and its excellent catalytic activity for reduction of organic dyes, *J. Alloy Compd.*, 719, 82-8, **2017**.

[59] Ismail M., Khan MI., Khan S.B., Akhtar K., Khan M.A., Asiri A.M., Catalytic reduction of picric acid, nitrophenols and organic azo dyes via green synthesized plant supported Ag nanoparticles, *J. Mol. Liq.*, 268, 87-101, **2018**.

[60] Choudhary M.K., Kataria J., Sharma S., Evaluation of the kinetic and catalytic properties of biogenically synthesized silver nanoparticles, *J. Clean Prod.*, 882-890, **2018**.

[61] Naseem K., Farooqi Z.H., Begum R., Irfan A., Removal of Congo red dye from aqueous medium by its catalytic reduction using sodium borohydride in the presence of various inorganic nano-catalysts: A review, *J. Clean Prod.*, 187, 296-307, **2018**.

6. ACKNOWLEDGEMENTS

The authors would like to thank Vellore Institute of Technology (VIT), Vellore 632014, India for the financial support and instrument facility to do this research work.

© 2018 by the authors. This article is an open access article distributed under the terms and conditions of the Creative Commons Attribution license (<http://creativecommons.org/licenses/by/4.0/>).